



City Research Online

City, University of London Institutional Repository

Citation: Guo, L., Liu, Y., Fu, F. & Huang, H. (2019). Behavior of axially loaded circular stainless steel tube confined concrete stub columns. *Thin-Walled Structures*, 139, pp. 66-76. doi: 10.1016/j.tws.2019.02.014

This is the accepted version of the paper.

This version of the publication may differ from the final published version.

Permanent repository link: <https://openaccess.city.ac.uk/id/eprint/21730/>

Link to published version: <https://doi.org/10.1016/j.tws.2019.02.014>

Copyright: City Research Online aims to make research outputs of City, University of London available to a wider audience. Copyright and Moral Rights remain with the author(s) and/or copyright holders. URLs from City Research Online may be freely distributed and linked to.

Reuse: Copies of full items can be used for personal research or study, educational, or not-for-profit purposes without prior permission or charge. Provided that the authors, title and full bibliographic details are credited, a hyperlink and/or URL is given for the original metadata page and the content is not changed in any way.

City Research Online:

<http://openaccess.city.ac.uk/>

publications@city.ac.uk

Behavior of axially loaded circular stainless steel tube confined concrete stub columns

Lanhui Guo^a*, Feng Fu^b, Yong Liu^a, Haijia Huang^a

^a School of Civil Engineering, Harbin Institute of Technology, Harbin, China

^b School of Mathematics, Computer Science & Engineering, City, University of London, EC1V 0HB, U.K.

Abstract: A stainless steel tube confined concrete (SSTCC) stub column is a new form of steel-concrete composite column in which the stainless steel tube without bearing the axial load directly is used to confine the core concrete. It could take the advantages of both the stainless steel tube and the confined concrete columns. This paper presents the experimental investigation of circular SSTCC stub columns subjected to axial load. Meanwhile, comparative tests of the circular concrete-filled stainless steel tubes and circular hollow stainless steel tubes were also conducted. The experimental phenomena of specimens are introduced in detail and the experimental results are analyzed. Through the investigation of axial stress and circumference stress on the stainless steel tube, the interaction behavior between stainless steel tube and core concrete is studied. The experimental results showed that the stainless steel tube provides better confinement to the concrete core, thus results the compressive capacity increased obviously comparing with unconfined concrete. The load-carrying capacity of SSTCC stub columns is higher than that of concrete-filled stainless steel tubes. An equation to calculate the load-carrying capacity of SSTCC stub columns was proposed, the results based on calculation are close to the experimental results.

Keywords: Stainless steel tube; steel tube confined concrete; stub columns; axially loaded; experimental study.

* Corresponding author.
E-mail address: guolanhui@hit.edu.cn

23 Notations

A_c	Cross-sectional area of the concrete core
A_s	Cross-sectional area of stainless steel tube
D	Out-diameter of stainless steel tube
E_s	Elastic modulus of stainless steel
E_s^t	Tangent modulus on the plastic stage of stainless steel
f_{cu}^{100}	Compressive strengths of 100 mm concrete cubes
f_{ck}	Compressive strengths of 150 mm concrete cubes
f_r'	Effective confining stress of circular tube on the concrete
f_p	Yield stress of stainless steel
N_s	Axial force on stainless steel tube
N_c	Axial force resisted by core concrete
N_{ue}	Ultimate compressive strength of specimen
t	Thickness of stainless steel tube
$\sigma_{0.2}$	Stress in accordance to 0.2% of plastic strain for stainless steel
σ_h	Hoop stress on stainless steel tube
σ_v	Vertical stress on stainless steel tube
σ_z	Equivalent stress on stainless steel tube
ε_h	Hoop strain on stainless steel tube
ε_v	Vertical strain on stainless steel tube
μ_s	Poisson's ratio of stainless steel
μ_{sp}	Poisson's ratio for the stainless steel in the plastic stage

24 **1. Introduction**

25 The conventional carbon steel tube confined concrete columns is a type of steel-concrete composite
26 column, in which the steel tube is discontinuous at the beam-column joints to ensure no axial load is
27 imposed directly to the tube [1-3]. Fig.1 shows the steel tube confined concrete columns. Concrete-filled
28 steel tubes as a kind of composite column are widely studied and used in the buildings. The main difference
29 between steel tube confined concrete columns and concrete filled steel tubes is that the steel tube is cut at
30 both end near to beam column connection for steel tube confined concrete members. If the steel tube is cut

31 on both ends, the steel tube would not resist the vertical load directly, thus the confinement to the core
32 concrete is better than that of concrete-filled steel tubes. Meanwhile, for steel tube confined concrete
33 columns, the beam-column connection is easy for the construction of rebar and pouring concrete if
34 reinforced concrete beam is applied. During the past decades, sufficient researches [4-8] have been
35 conducted on the behaviors of the steel tube confined concrete columns, which indicates that such type of
36 members has relatively high bearing capacity, good ductility as well as excellent fire resistance. In addition,
37 the steel tube can act as the formwork during the construction stage, making it easier to cast the concrete.
38 Due to the excellent mechanical and manufacture properties, steel tube confined concrete columns are used
39 increasingly in projects, especially in the Middle East and the east Asia. Fig.2 shows the application of
40 circular steel tube confined concrete columns used in Zhongke Tower, Chongqing. This 26-storey building
41 will be finished in 2019. The height of this building is 99.80 m.

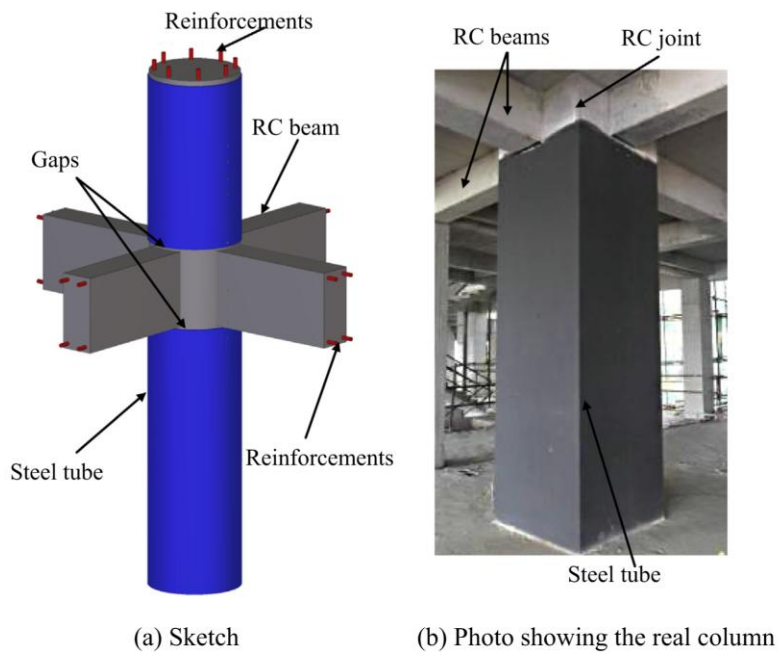


Fig.1. Steel tube confined concrete columns

42

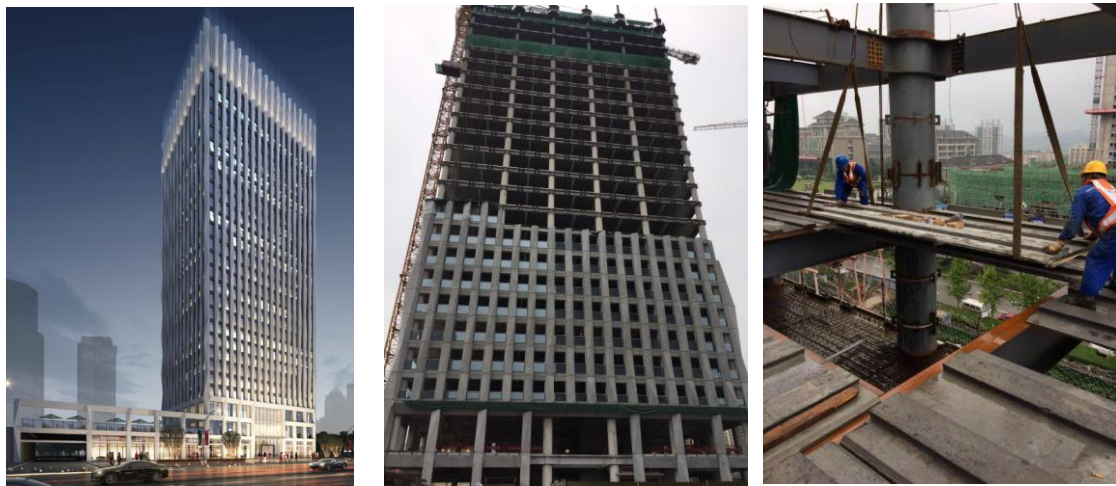


Fig.2. Zhongke Tower

43 Using stainless steel tube is another innovation for steel tube confined concrete columns. Apart from
44 the advantages mentioned above, the stainless steel tube confined concrete (SSTCC) columns also have the
45 extra benefits such as the fine aesthetic appearance and high corrosion resistance associated with the
46 material of stainless steel. Unlike carbon steel, stainless steel possesses natural corrosion resistance. Thus,
47 after being appropriately processed, the surface can be exposed without any protective coatings. Besides,
48 stainless steel also exhibits features, such as the ease of maintenance, ease of construction and high fire
49 resistance compared to traditional carbon steel. Therefore, stainless steel could be used in steel tube
50 confined concrete column to enhance its durability.

51 In the past, experimental and theoretical studies have been conducted on the behaviors of carbon steel
52 tube confined concrete columns, which included axially loaded behavior, eccentric loaded behavior and
53 seismic behavior. The square and circular shape cross-sections were both studied. Based on these studies,
54 the methods to calculate loading-carrying capacities of carbon steel tube confined concrete columns were
55 proposed [9-11].

56 Compared to the carbon steel, stainless steel has a stress-strain curve with no yield plateau and low
57 proportional limit stress. The ductility of stainless steel is much better than that of carbon steel. Because of

58 the advantageous and different properties of stainless steel, some researchers such as Young and Elloboldy
59 [12-14] studied the behavior of concrete-filled stainless steel tube (CFSST) columns. A series of tests were
60 conducted to investigate the effects of the shape of stainless steel tube, plate thickness and concrete strength
61 on the behavior and strength of axially loaded CFSST columns. Dennis and Leroy [15] tested eight CFSST
62 columns and eight concrete filled carbon steel tube columns with square section. They also compared the
63 strengths of those members with that determined by the existing design methods for composite carbon steel
64 sections in Eurocode 4 and ACI 318. In addition, a new method to predict the axial capacity of concrete
65 filled stainless steel hollow sections was also developed. In 2013, Hassanein et al. [16] performed finite
66 element analysis on the behavior of CFSST columns. Suliman et al [17] tested thirty-five concrete-filled
67 stainless steel tubular columns to investigate the effect of different parameters on their behavior. Two
68 concrete compressive strengths of 44 MPa and 60 MPa and three diameter-to-thickness ratios of 54, 32, and
69 20 were considered. The axially loaded behavior of concrete-filled stainless/carbon steel double skin
70 columns were done by Ye, Han and Wang [18-20]. Feng and Chen did a series of research works about
71 CFSST columns, which includes the bond behavior between tube and concrete and the flexural behavior of
72 the members [21-24].

73 The above literature review indicates that past studies were mainly focused on carbon steel tube
74 confined concrete columns or concrete-filled stainless steel tube columns. Currently, little research has been
75 conducted on SSTCC columns. As it has been discussed, stainless steel can be used to replace carbon steel
76 for enhancing the durability of steel tube confined concrete columns. However, limited experimental
77 investigations were presented in available literatures focusing on the performance of axially loaded SSTCC
78 columns.

79 To understand the behavior of SSTCC columns clearly, a series of tests were conducted under axial

80 compression. For comparison purposes, concrete-filled stainless steel tubular columns and hollow stainless
81 steel tubes were tested. At last, an equation to calculate the load-carrying capacity of SSTCC columns
82 subjected to axial load was suggested.

83 **2. Experimental study**

84 *2.1. Test specimens*

85 In order to understand the behaviors of stainless steel tube confined concrete (SSTCC) columns, 18
86 specimens were tested under monotonic loaded axial compression load using the 5000 kN capacity
87 high-stiffness compression machine at the structural lab in Harbin Institute of Technology. Among 18
88 specimens, nine of them are stainless steel tube confined concrete stub columns, six specimens are concrete
89 filled stainless steel stub columns, and three specimens are hollow stainless steel tubes columns. All
90 specimens are stub columns with a height-to-diameter ratio of 3.0 to eliminate the end effect and column
91 slenderness effect. The dimensions of all specimens are presented in Fig. 3 and Table 1. Two kinds of
92 thicknesses of steel plate are selected, which are 1.3 mm and 1.65 mm. The diameter-to-thickness ratio
93 varies from 89 to 109.

94 All the tubes employed were produced by rolling the steel plate to circular members, and then weld
95 the steel tube by butt weld. A rigid end plate with 10 mm thickness was welded to the bottom of the tube.
96 The concrete was filled into the tube and after 28 days of curing, another rigid steel pate was covered and
97 welded to the top of the tube. The surface of end plates was smooth and flat after grinding using a grinding
98 wheel with diamond cutters. This was to ensure that the load was applied evenly across the cross-section
99 and simultaneously to the steel tube and the core concrete. To insure the axial load is applied to the core
100 concrete only in SSTCC columns, two 10 mm wide girth strips were cut off from the steel tube at 30 mm
101 away from the end plates, as shown in Fig. 3.



(a) Concrete filled stainless steel tube columns (b) Stainless steel tube confined concrete members

Fig.3. Dimension of the specimen

102
103

Table 1 Geometric and material properties of specimens

Specimens	H /mm	D /mm	t /mm	D/t	$\sigma_{0.2}$ /MPa	f'_c /MPa
SSTCC-D125-a	374.5	125.3	1.29	97	496	54.5
SSTCC-D125-b	374.9	124.8	1.25	100	496	54.5
SSTCC-D125-c	374.8	124.5	1.33	94	496	54.5
CFSST-D125-a	375.3	124.8	1.31	95	496	54.5
CFSST-D125-b	374.5	125.3	1.30	96	496	54.5
SST-D125-a	375.5	124.8	1.31	96	496	--
SSTCC-D150-a	444.9	149.7	1.63	92	493	54.5
SSTCC-D150-b	444.8	149.8	1.67	90	493	54.5
SSTCC-D150-c	445.1	150.2	1.67	90	493	54.5
CFSST-D150-a	444.8	150.1	1.68	89	493	54.5
CFSST-D150-b	444.9	149.8	1.65	91	493	54.5
SST-D150-a	445.0	150.2	1.66	90	493	--
SSTCC-D180-a	540.4	180.8	1.68	108	493	54.5
SSTCC-D180-b	540.5	180.6	1.65	109	493	54.5
SSTCC-D180-c	539.8	180.7	1.67	108	493	54.5
CFSST-D180-a	539.7	180.7	1.69	107	493	54.5
CFSST-D180-b	540.4	180.7	1.70	106	493	54.5
SST-D180-a	539.9	180.8	1.70	106	493	--

104 Note: In the nomenclature of the group, ‘SSTCC’ is the abbreviation of circular stainless steel tube confined
 105 concrete; ‘CFSST’ is the abbreviation of circular concrete-filled stainless steel tubes; ‘SST’ is the abbreviation of
 106 circular hollow section stainless steel tubes. “D125” means the nominal diameter of the specimen is 125 mm
 107 while “a” is the number for the specimen of the same type.

108

109 *2.2. Material properties*

110 The stainless steel employed in the specimen is the austenitic stainless steel with the section of ASTM
111 (American Society for Testing and Materials) 304. In order to determine the property of stainless steel,
112 three tensile coupons were cut from a randomly location of the selected steel sheet. The coupons were made
113 and tested in accordance with the Chinese standard GB/T 228-2002 [25]. Typical tensile stress-strain curve
114 of stainless steel is presented in Fig. 4. As can be seen, the stress-strain curve of the stainless steel has no
115 yield plateau and good ductility.. For steel plates with thickness of 1.3 mm and 1.65 mm, the elastic
116 modulus of steel plates were $2.17 \text{ E}+5 \text{ N/mm}^2$ and $2.15 \text{ E}+5 \text{ N/mm}^2$, and the average yielding strengths
117 were 496 N/mm^2 and 493 N/mm^2 , respectively.

118 When casting concrete, three concrete prisms with dimension of $150 \text{ mm} \times 150 \text{ mm} \times 300 \text{ mm}$ were
119 casted and cured in the same conditions as the specimens. The test procedure was in accordance to the
120 Chinese standard GB/T 50081-2002 [26]. The average compressive strength of concrete was 54.5 N/mm^2 .
121 The average modulus of concrete was 38100 N/mm^2 .

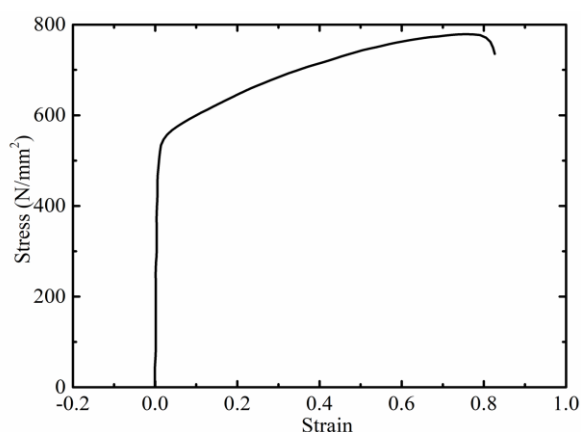


Fig.4. Strain-stress relationship of stainless steel with thickness of 1.3 mm

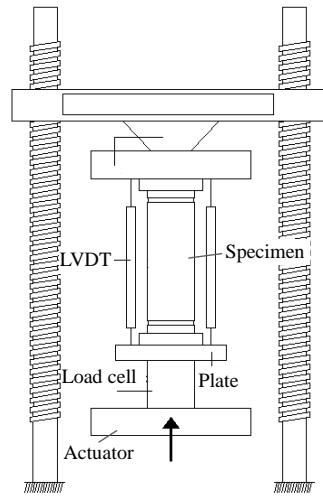
122 *2.3. Experimental setup and load schedule*

123 As shown in Fig. 5 and Fig. 6, eight strain gauges were stuck at the mid-height on each face of the
124 specimen, which were arranged in the longitudinal and transverse directions with 90° angles. Four

125 displacement transducers were used to measure the axial deformation. Fig. 5 illustrates the experimental
 126 setup.



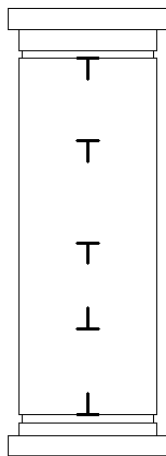
(a) Photo of test setup



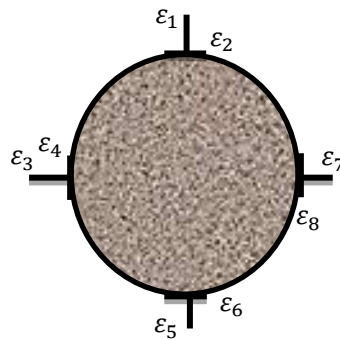
(b) Diagram of setup

Fig.5. Experimental setup

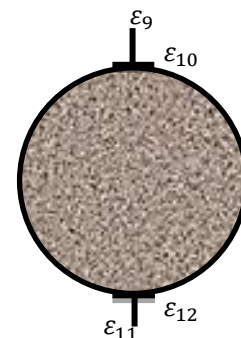
127 The tests were conducted using a 5000 kN capacity universal testing machine in Harbin Institute of
 128 Technology, and the load was applied directly on the specimen. The tests were firstly loaded with
 129 controlled increment of the rate of 0.06MPa/s. When the yielding of specimen starts (the maximum strain
 130 reaches the yielding strain of steel plate), the loading process turned into the displacement control with the
 131 rate of 10 $\mu\text{e/s}$. The tests were terminated when the axial load decreased to 75% of the peak load caused by
 132 fracture of steel plate or crushing of concrete.



(a) Side view of columns



(b) Section at mid-height



(c) End and quartile section

Fig.6. Location of strain gauges

133 **3. Experimental phenomena**

134 *3.1. Stainless steel tube confined concrete stub columns*

135 During the initial loading stage, no significant changes were observed. Before the axial load reached 80%
136 of peak load, the relationship between axial load and deformation was kept as linear, and the specimen was
137 in the elastic stage. After the load exceeded 80% of peak load, the axial displacement started to quickly
138 increase with the increasing of axial load. When the axial load reached 98% of peak load, small cracking
139 appeared at the position of cutting of steel tube. When the specimen reached the peak load, the concrete at
140 the cutting position of steel tube spalled. Then the axial load decreased slowly with the increasing of axial
141 deformation. When the axial load decreased to 85% of peak load, the lateral deflection of steel tube was
142 observed, and the steel tube was slightly bloated without significant local buckling. To observe the damage
143 of core concrete, the steel tubes were cut off and removed after the test. It is noticed that the core concrete
144 fails in shear failure mode with severe cracks along the diagonal direction. The angle between shear failure
145 plane and the horizontal direction is about 45°~49°. The experimental phenomena of typical specimens are
146 shown in Fig.7. For specimens with diameter of 150 mm, when the axial load decrease to 93% from the
147 peak load, the steel tube at the position of welding broke, thus the load started to decrease sharply. The
148 reason was that the steel tube cannot provide confinement to the core concrete any more. Therefore, it is
149 noticeable that, the quality of longitudinal weld is very important for this type of structural members,
150 especially for the sake of sufficient ductility of the specimen.

151



(a) Phenomena of specimen SSTCC-D125-a

(b) Phenomena of specimen SSTCC-D150-b

Fig.7. Failure mode of stainless steel tube confined concrete members

152 *3.2. Concrete-filled stainless steel tubular columns*

153 For concrete-filled stainless steel tubular columns, the phenomena of all specimens were similar to
 154 each other. Taken specimen CFSST-D125-b as an example, the phenomena and failure mode were
 155 introduced in the following. Before the axial load reached 80% of peak load, there was no evident
 156 phenomenon on the surface of the specimen. The relationship between axial load and vertical deformation
 157 kept linear. When the specimen reached 80% of peak load, the stiffness of axial load-deformation
 158 relationship curve began to decrease. The local bulge of steel tube was observed near the bottom (about 50
 159 mm from end plate). The bulge gradually increased with the increase of vertical deformation. The peak load
 160 of the specimen was 1142 kN, and the corresponding vertical displacement was 2.72 mm. When the
 161 specimen decreased to 95% of peak load, the steel tube bloated at the mid-height position. When the axial
 162 load decreased to 90% of peak load, the axial load decreased very slowly with the increase of vertical
 163 deformation. The specimen exhibited global shear failure mode. The angle between shear failure plane and
 164 horizontal plane was located between 48°~53°. The experimental phenomena were shown in Fig. 8.



(a) Phenomena of specimen CFSST-D125-a (b) Phenomena of specimen CFSST-D150-b

Fig. 8 Failure mode of concrete-filled stainless steel tubes

165 *3.3. Hollow stainless steel tubes with circular section*

166 According to the Eurocode 3 ‘Design of Steel Structures, Part 1-4: General rules-Supplementary rules
 167 for stainless steels’, if the diameter-to-thickness ratio (D/t) ratio is over $90 \cdot 235 / \sigma_{0.2} \cdot E_s / 210000$, the local
 168 buckling would appear for circular hollow stainless steel sections before the steel reaches its yielding
 169 strength. According to the Chinese Technical specification for stainless steel structures, if the diameter to
 170 thickness ratio is over $100 \cdot 235 / \sigma_{0.2}$, the local buckling of circular hollow section stainless steel stub would
 171 be considered. Considering the yielding stress of stainless steel of 493 N/mm^2 , the limit
 172 diameter-to-thickness ratios for local buckling are 42.9 and 47.7 according to EC 3 code and Chinese
 173 design code, respectively. In the test, for specimens with diameter of 125 mm, 150 mm and 180 mm, the
 174 corresponding diameter-to-thickness ratios are 96, 90 and 106, respectively. It can be seen that the circular
 175 stainless steel tube would fail in the elastic stage.

176 For stainless steel hollow section, at the initial loading stage, there is no evident phenomenon for these
 177 specimens. The axial load-deformation relationship kept linear before the specimens reached 80% of their
 178 bearing capacity. Beyond this, the deformation increased significantly with the increase of axial load. The
 179 rigidity of axial load-deformation relationship curve began to decrease. When the specimen reached its

180 peak load, the inward local buckling near the bottom occurred accompanied by a sudden drop of the
181 load-carrying capacity and the increase of vertical displacement. The reason was that the specimen failed at
182 the elastic stage of steel. From these specimens, it can be seen that severe buckling ripples appeared on the
183 steel tubes. The experimental phenomena are shown in Fig. 9. When the load dropped to 50% of peak load,
184 the vertical deformation reached the 1/50 of the specimen height. The test was terminated.



Fig.9. Experimental phenomena of stainless steel tubes with circular hollow section

185 **4. Experimental results analysis**

186 *4.1. Interaction behavior between steel tube and core concrete*

187 *4.1.1. Strain-stress relationship of stainless steel under biaxial stresses*

188 In 2008, Quach, Teng and Chung [27] developed three-stage strain stress relationship formula which is
189 based on the extensive theoretical and experimental research works. In this paper, the authors further
190 modified the formula based on the regression of the test results of stainless steel coupons presented in this
191 paper. The modified formulae are coincided well with the strain-stress relationship of stainless steel. The
192 formulae are as follows:

193

194

195

$$\varepsilon = \begin{cases} \sigma/E_s & (\sigma \leq f_p) \\ \frac{\sigma}{E_s} + 0.002 \left(\frac{\sigma}{\sigma_{0.2}} \right)^n & (f_p < \sigma \leq \sigma_{0.2}) \\ \frac{\sigma - \sigma_{0.2}}{E_s} + \left[0.008 + (\sigma_{1.0} - \sigma_{0.2}) \left(\frac{1}{E_s} - \frac{1}{E_{0.2}} \right) \right] & (\sigma_{0.2} < \sigma \leq \sigma_{1.0}) \\ \left(\frac{\sigma - \sigma_{0.2}}{\sigma_{1.0} - \sigma_{0.2}} \right)^{n'_{0.2,1.0}} + \varepsilon_{0.2} & \\ \frac{\sigma - \sigma_{1.0}}{k_2 E_s} + \varepsilon_{1.0} & (\sigma > \sigma_{1.0}) \end{cases} \quad (1)$$

196 Where, ε is the strain of stainless steel;

197 σ is the stress of stainless steel;

198 E_s is the initial elastic modulus of stainless steel;

199 f_p is the yield stress of stainless steel, and $f_p = k_1 \sigma_{0.2}$;

200 $\sigma_{0.2}$ is the nominal yield stress in accordance to 0.2% plastic strain;

201 $E_{0.2}$ is the tangent modulus corresponding to nominal yield stress of $\sigma_{0.2}$, $\frac{E_{0.2}}{E_s} = \frac{1}{1 + 0.002n/e}$;

202 n is the strain hardening index, $n = \frac{\ln(20)}{\ln(\sigma_{0.2}/\sigma_{0.01})}$;

203 e is the coefficient, $e = \frac{\sigma_{0.2}}{E_s}$;

204 For stainless steel, k_1 is taken as 0.35, k_2 is taken as 0.02;

205 $\sigma_{1.0}$ is calculated according to $\sigma_{1.0}/\sigma_{0.2} = 0.542/n + 1.0$.

206 The stress analysis method from reference [28] is used in this paper. Different to CFSST, for SSTCC
 207 columns, the stainless steel tube would confine the lateral expansion of core concrete. In reality, the stress
 208 in radial direction of stainless steel tube is very small, which can be neglected. Thus, the stainless steel tube
 209 is assumed to be under the state of hoop tensile stress combining with axial compressive stress. According
 210 to the lateral and longitudinal strain of the stainless steel tube obtained from the tests, the axial stress σ_v ,
 211 hoop stress σ_h and equivalent stress σ_z on the stainless steel tube can be calculated based on the

212 assumptions that:

- 213 • the stress in the radial direction of the tube is ignored;
- 214 • thin plate theory is used for the tube, therefore, the circumference stress is presumed evenly
- 215 distributed along the thickness of the wall;
- 216 • the concrete core is under the axial and radius stress states;
- 217 • no slips are presumed between the tube and the concrete core.

218 The stress-strain relationships of stainless steel for each stage is as follows:

219 1) In the elastic stage, the stainless steel follows the Hooke's Law:

$$220 \begin{bmatrix} \sigma_h \\ \sigma_v \end{bmatrix} = \frac{E_0}{1-\mu_s^2} \begin{bmatrix} 1 & \mu_s \\ \mu_s & 1 \end{bmatrix} \begin{bmatrix} \varepsilon_h \\ \varepsilon_v \end{bmatrix} \quad (2)$$

221 Where, μ_s is the Poisson's ratio for stainless steel.

222 2) In the plastic stage, the stainless steel follows Elastic-Plastic theory:

$$223 \begin{bmatrix} \sigma_h \\ \sigma_v \end{bmatrix} = \frac{E_s^t}{1-\mu_{sp}^2} \begin{bmatrix} 1 & \mu_{sp} \\ \mu_{sp} & 1 \end{bmatrix} \begin{bmatrix} \varepsilon_h \\ \varepsilon_v \end{bmatrix} \quad (3)$$

224 Where, E_s^t is the secant modulus.

$$225 E_s^t = \begin{cases} 1 / \left[\frac{1}{E_0} + \frac{0.002n \left(\frac{\sigma}{\sigma_{0.2}} \right)^{n-1}}{\sigma_{0.2}} \right] & f_p \leq \sigma < \sigma_{0.2} \\ 1 / \left[\frac{1}{E_{0.2}} + \frac{\left[0.008 + (\sigma_{1.0} - \sigma_{0.2}) \left(\frac{1}{E_0} - \frac{1}{E_{0.2}} \right) \right] n'_{0.2} \cdot 1.0 \left(\frac{\sigma - \sigma_{0.2}}{\sigma_{1.0} - \sigma_{0.2}} \right)^{n-1}}{\sigma_{1.0} - \sigma_{0.2}} \right] & \sigma_{0.2} \leq \sigma \leq \sigma_{1.0} \end{cases} \quad (4)$$

226 μ_{sp} is the Poisson's ratio of stainless steel in the plastic stage,

$$227 \mu_{sp} = 0.167 \frac{\sigma_p^f}{f_y f_p} + 0.283 \quad (5)$$

228 3) In the strain hardening stage

$$229 \begin{bmatrix} \sigma_h \\ \sigma_v \end{bmatrix} = \frac{E_s}{Q} \begin{bmatrix} \sigma_v'^2 + 2p & -\sigma_v' \sigma_h' + 2\mu_s p \\ -\sigma_v' \sigma_h' + 2\mu_s p & \sigma_h'^2 + 2p \end{bmatrix} \begin{bmatrix} \varepsilon_h \\ \varepsilon_v \end{bmatrix} \quad (6)$$

230 Where, σ_v' is the axial stress, $\sigma_v' = \sigma_v - \sigma_{cp}$;

231 σ_h' is the circumference stress, $\sigma_h' = \sigma_h - \sigma_{cp}$;

232 σ_{cp} is the average stress, $\sigma_{cp}=1/3 (\sigma_h + \sigma_v)$;

233
$$p = \frac{2H'}{9E_s} \sigma_z^2 \quad (7)$$

234
$$H' = \frac{d\sigma}{d\epsilon_p} = 10^{-3} E_s^2 \quad (8)$$

235 σ_z is the equivalent stress, $\sigma_z = \sqrt{\sigma_h^2 + \sigma_v^2 - \sigma_h \sigma_v}$;

236
$$Q = \sigma_h^2 + \sigma_v^2 + 2\mu_s \sigma_h \sigma_v + \frac{2H'(1-\mu_s)}{9G} \sigma_z^2;$$

237 When the stress such as σ_v , σ_h and σ_z are calculated, the internal force of the tube and the concrete core
238 can be calculated correspondingly.

239 The axial force resisted by the stainless steel tube N_s :

240
$$N_s = \sigma_v A_s \quad (9)$$

241 Where, A_s is the cross-sectional area of the tube; σ_v is the axial stress of the tube.

242 The axial stress of the concrete σ_c can also be derived as

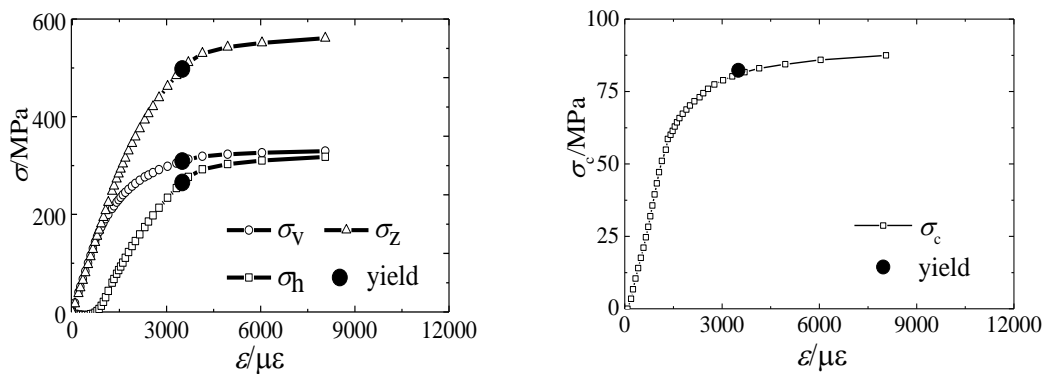
243
$$\sigma_c = (N - N_s) / A_c \quad (10)$$

244 Where, N is the axial load of the specimen; A_c is the cross-sectional area of core concrete.

245 4.1.2. Interaction behaviour of stainless steel tube and core concrete for SSTCCs

246 Based on the above calculation method, the vertical stress and horizontal stress on the stainless steel
247 tube for SSTCC members can be calculated. Fig. 10 shows the average stress and strain relationship curves
248 at the mid-height of the specimen. In Fig. 10 (a), the symbol σ_v denotes the axial average stress, the symbol
249 σ_h denotes the circumference stress, and the σ_z denotes the equivalent stress. For comparison of the values,
250 the axial stress σ_v (compressive stress) defines as positive values. In the elastic stage, the axial stress σ_v
251 increased with the increasing of axial strain, and the circumference stress σ_h is nearly about zero. The axial
252 stress is resulted from the friction between steel tube and core concrete. Thus the steel tube at the
253 mid-height of the specimen would resist the axial stress. The mechanism of SSTCC column is similar to
254 that of the concrete-filled steel tube columns. In this stage, the circumference deformation of concrete is

255 very small and the interaction behavior between stainless steel tube and concrete is not obvious. When the
 256 axial strain ε_v reached 850 $\mu\varepsilon$, the corresponding stress of core concrete was equal to 39.4 MPa. At this
 257 point, the average stress of core concrete reached the compressive strength of concrete. Beyond this point,
 258 the circumference stress increased sharply with the increasing of axial strain. When the equivalent stress
 259 reached the stress of $\sigma_{0.2}$, the corresponding axial stress and circumference stress are 309 MPa and 265
 260 MPa, respectively. Under different strain level, the load resisted by the steel tube can be calculated, then the
 261 load resisted by the core concrete can be calculated by subtracting the load resisted by stainless steel tube
 262 from the total axial load. Fig. 10 (b) shows the average axial strain-stress relationship curve of core
 263 concrete. It can be seen that when the steel tube reached its yielding stress, the average compressive stress
 264 of core concrete reached 85 MPa, which is much higher than the maximum compressive stress of 54.5 MPa
 265 of unconfined concrete. This is due to the tube confinement to the core concrete.



(a) Axial stress vs. strain on stainless steel tube (b) Axial stress vs. strain of the core concrete

Fig.10. Average stress and strain relationship curves of specimen SSCCT-D125-a

266 4.1.3. Interaction behaviour of stainless steel tube and core concrete for CFSSTs

267 The axial stress-strain relationship curves on the stainless steel tube of concrete-filled stainless steel
 268 tubes are shown in Fig. 11 (a). It can be seen that the axial stress of steel is almost same to the equivalent
 269 stress when the axial strain of steel is less than 3000 $\mu\varepsilon$. In addition, the circumference stress of steel is

270 negative value, which means the steel tube is under compression along the circumference direction. The
 271 reason was that the Poisson's ratio of concrete is smaller than that of steel. The radial deformation of steel
 272 is larger than that of concrete. However, the cohesion between steel and concrete restrained the radius
 273 deformation of steel tube. Thus the circumference stress of steel tube appeared as axial stress. With the
 274 increasing of axial strain, the Poisson's ratio of concrete became larger than that of steel. The expansion
 275 deformation of core concrete became larger than that of steel. The stainless steel tube would confine the
 276 deformation of core concrete. When the equivalent stress reached the yield stress of stainless steel, the
 277 circumference stress on the steel tube is 50 MPa. The core concrete is under the state of three-directional
 278 compression. The compressive stress of core concrete reached 75 MPa, which is higher than that of
 279 concrete without confinement. Besides, the compressive stress of core concrete in CFSST columns is
 280 smaller than that in SSTCC columns indicating that the confinement of stainless steel tube in CFSST
 281 columns is smaller than that in SSTCC columns.

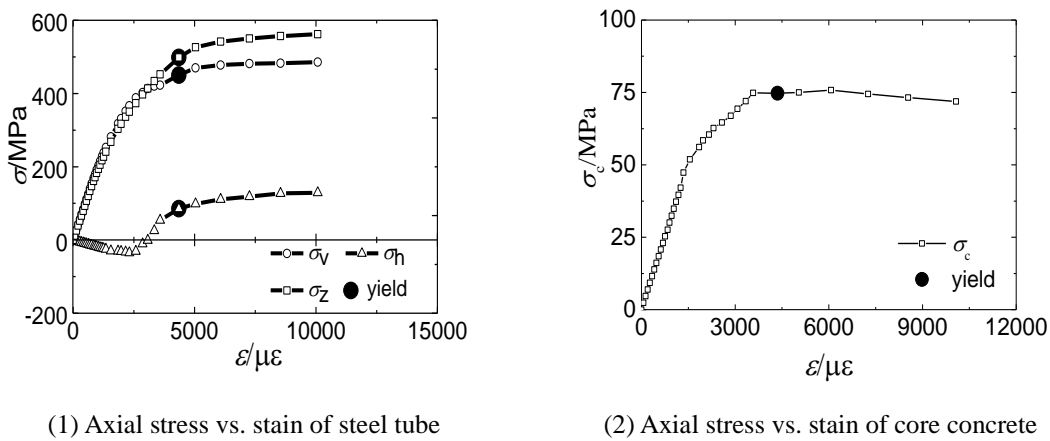


Fig.11. Average stress and strain relationship curves of specimen CFSST-D150-1

282 *4.2. Axial load-strain relationship curves*

283 Fig. 12 and Fig. 13 show the axial load-strain relationship curves of SSTCC stub columns and CFSST.
 284 For SSTCC stub columns, the axial strain is defined as the axial deformation divided by the height of the
 285 specimen. It can be seen that the rigidity and load-carrying capacity of each group of specimens with same

286 parameters are close to each other. The deformation ability of CFSST stub columns is better than that of
 287 SSTCC stub columns. The reason was that the circumference stress of SSTCC stub columns is larger than
 288 that of CFSST columns. The failure of the welding on SSTCC stub columns resulted in the early failure of
 289 the specimens. Hence, for SSTCC columns, the hot-rolled stainless steel tubes are suggested to be used in
 290 the construction.

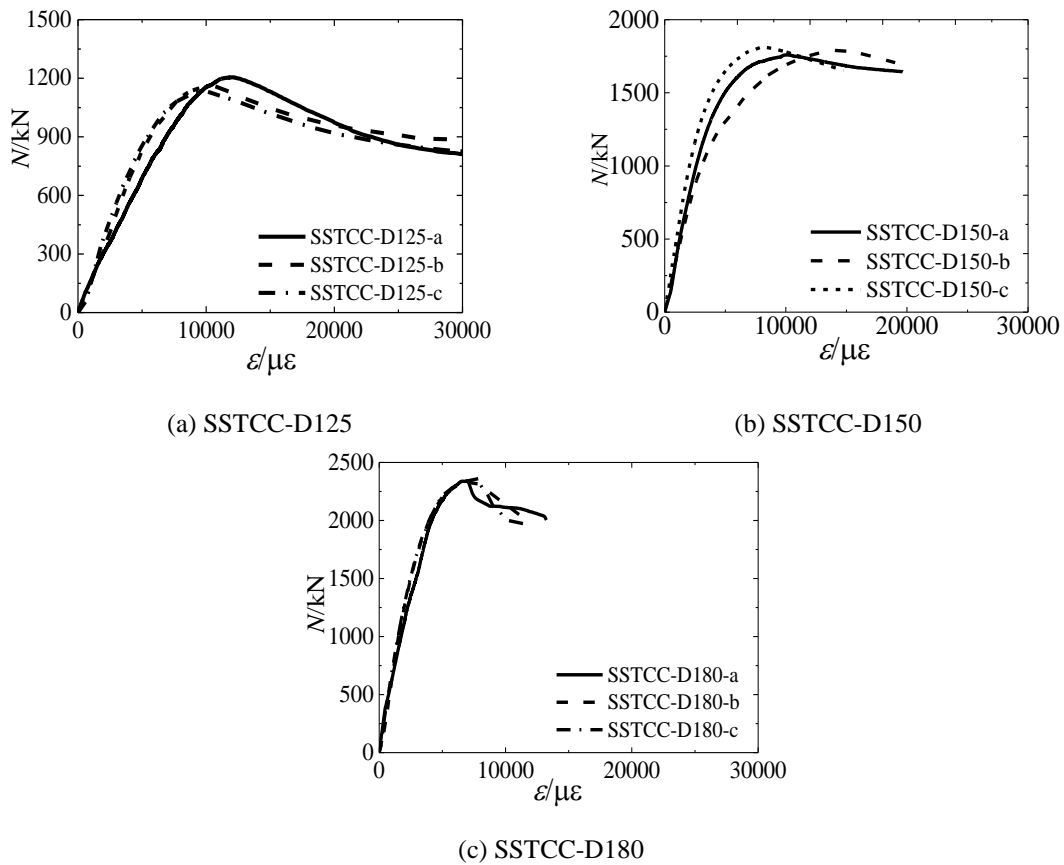
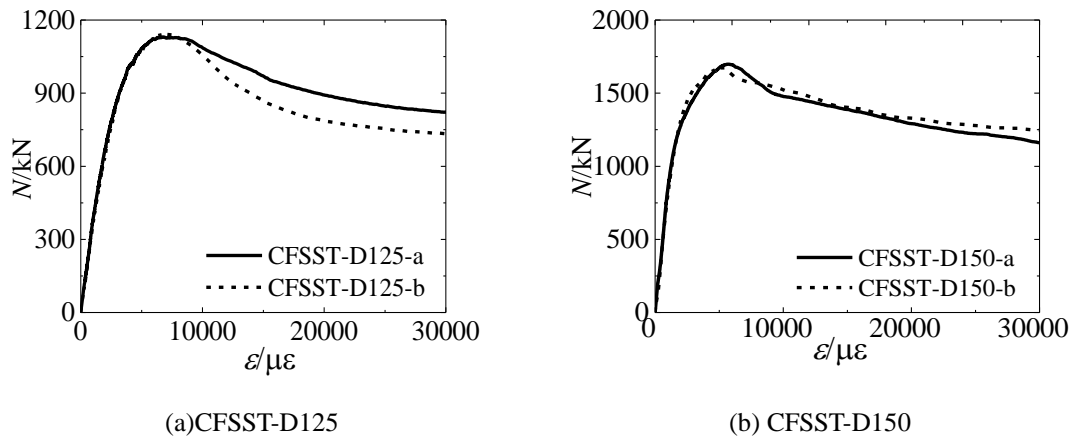
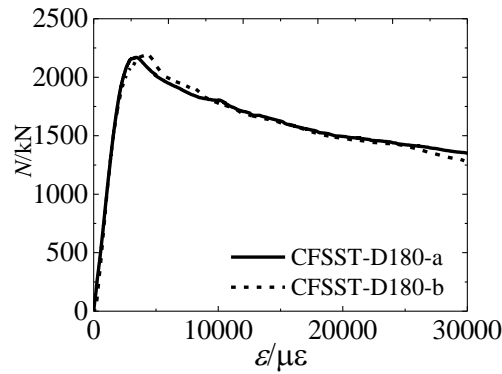


Fig. 12. Axial strain vs. axial load relationship of SSTCC stub columns





(c) CFSST-D180

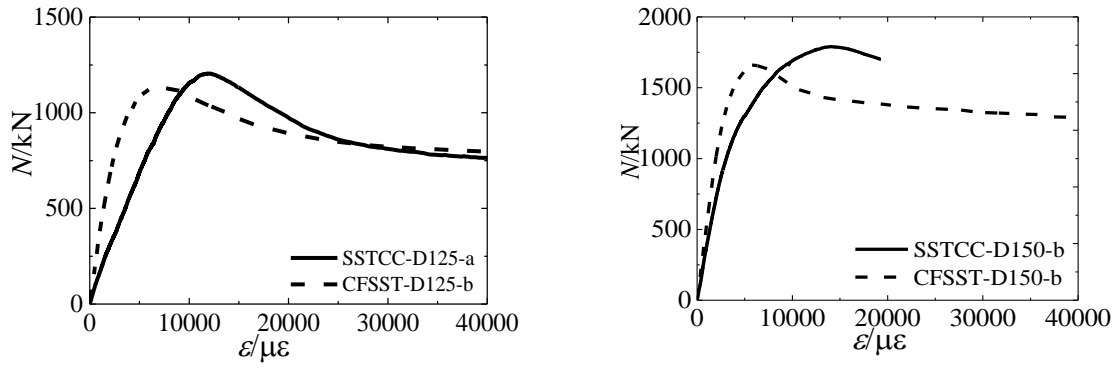
Fig.13. Axial strain and load relationship of CFSST stub columns

291 *4.3. Comparison of experimental results*

292 Fig. 14 shows the comparison of SSTCC columns and CFSST columns with same diameter. For
 293 SSTCC columns, the core concrete is subjected to compression and the stainless steel tube would not
 294 contribute to resist the vertical load directly. While for CFSST columns, the steel tube and core concrete are
 295 loaded simultaneously. From Fig. 14, it can be seen that the load-carrying capacity of SSTCC columns is
 296 higher than that of CFSST columns. For specimen with diameter-to-thickness ratios of 108, 97 and 90, the
 297 increase ratio of load-carrying capacity are 2.5%, 6.4% and 7.5%.

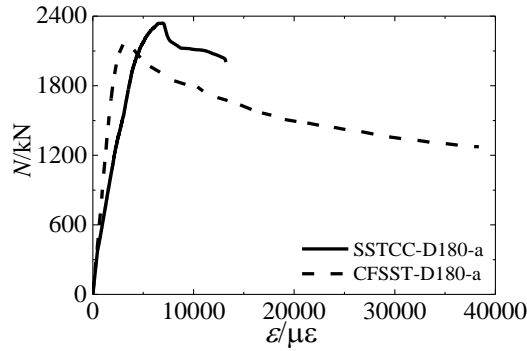
298 The rigidity of stainless steel tube confined concrete member is obviously lower than that of concrete-filled
 299 steel tubes. The rigidity of tube confined concrete member decreases about 20%. In addition, the
 300 deformation corresponding to peak load of SSTCC column is larger than that of CFSST column. For tube
 301 confined concrete member, in elastic stage, the steel tube has little contribution to the rigidity. While for
 302 CFSST columns, the steel tube is mainly to resist vertical load in elastic stage. In the elastic-plastic stage,
 303 the hoop stress of tube increases which would decrease the axial compressive stress of steel tube according
 304 to Von-Mises criterion.

305



(a) Specimens with diameter of 125 mm ($D/t=97$)

(b) Specimens with diameter of 150 mm ($D/t=90$)



(c) Specimens with diameter of 180 mm ($D/t=108$)

Fig.14. Comparison between SSTCC and CFSST

306 5. Axial strength of stainless steel tube confined stub columns

307 Although the stainless steel tube is not supposed to contribute to the axial resistant to the compressive
 308 loading, based on the experimental results, it was found that the stainless steel tube at the mid-height would
 309 partially resist the axial load even the stainless steel tube is cut on both ends. This is due to the friction
 310 between steel tube and core concrete, which enable the steel tube to take the axial load. The circumference
 311 stress on the steel tube would confine the concrete, thus the concrete was under the state of three-
 312 directional compression. The compressive strength of confined concrete was proposed by Mander [29]:

$$313 \quad f_{cc} = f_c' \left(-1.245 + 2.245 \sqrt{1 + 7.94 \frac{f_r'}{f_{co}'} - 2 \frac{f_r'}{f_{co}'}} \right) \quad (11)$$

314 Where, f_r' is the effective confining stress of circular tube on the concrete, which can be calculated as
 315 following:

316
$$f_r' = \frac{2t\sigma_h}{D-2t} \quad (12)$$

317 The stainless steel is also assumed to obey the Von-Mises yielding criterion as following:

318
$$\sigma_z = \sqrt{\sigma_h^2 + \sigma_v^2 - \sigma_h\sigma_v} \quad \text{and} \quad \sigma_z \leq \sigma_{0.2}$$

319 When the stainless steel reached the yielding stress, it can be assumed that the steel meets the
320 following equation.

321
$$\sigma_{0.2} = \sqrt{\sigma_h^2 + \sigma_v^2 - \sigma_h\sigma_v} \quad (13)$$

322 After the axial stress σ_v is known, the corresponding circumference stress σ_h can be calculated
323 according to Eq. (13).

324 Based on the test results of SSTCC columns, it was found that when the specimens reached their
325 load-carrying capacity, the axial stress on the steel tube is about 60% of yielding stress. According to the
326 Von-Mises criterion, the circumference stress on the steel tube is 0.55 times of yielding stress. Based on the
327 test results of CFSST columns, it was found that the axial stress on the steel tube is about 0.9 times of
328 yielding stress of steel when the specimens reached their load-carrying capacity, and the corresponding
329 circumference stress on the steel tube is 0.18 times of yielding stress. Thus the following equation is
330 suggested to calculate the loading-carrying capacity of stainless steel tube confined concrete stub columns
331 and concrete-filled stainless steel tube stub columns.

332
$$N_u = f_{cc}A_c + A_s\sigma_v \quad (14)$$

333
$$\sigma_v = \beta\sigma_{0.2} \quad (15)$$

334
$$\sigma_h = \frac{\sqrt{4-3\beta^2}-\beta}{2}\sigma_{0.2} \quad (16)$$

335 In which, β is the proportional factor of axial stress corresponding to the yielding stress of steel; f_{cc}
336 can be calculated by Eq. 11. A_c is the area of core concrete; A_s is the area of steel tube. As analyzed above,
337 the factor β is 0.6 for SSTCC columns while 0.9 for CFSST columns. Using the Eq. 14, the load-carrying

338 capacities of all specimens are calculated and listed in Table 2. It can be seen that the calculated results are
 339 close to the experimental results, indicating that the proposed equation can be used to calculate the
 340 load-carrying capacity of stainless steel tube confined concrete members and concrete-filled stainless steel
 341 tubes. Also, the capacities of sum of concrete and stainless steel tube are listed in Table 2. It can be seen
 342 that the capacity of SSTCC columns are about 34% higher in average than the sum of concrete and steel
 343 tube, while the capacity of CFSST columns are about 27% higher in average than the sum of concrete and
 344 steel tube. The reason is that the core concrete is confined by stainless steel tube in all columns and the
 345 confinement of stainless steel tube in SSTCC columns is larger than that in CFSST columns.

Table 2 Comparison between test results and calculated results

No.	D <i>mm</i>	t <i>mm</i>	Δ_u mm	N_{s+c} kN	N_{ue} kN	N_c kN	N_c/N_{ue}	N_{ue}/N_{s+c}
SSTCC-D125-a	125.3	1.29	3.59	905	1205	1174	0.974	1.33
SSTCC-D125-b	124.8	1.25	3.61	905	1160	1153	0.994	1.28
SSTCC-D125-c	124.5	1.33	3.63	905	1131	1175	1.039	1.25
CFSST-D125-a	124.8	1.31	2.72	905	1131	1047	0.926	1.25
CFSST-D125-b	125.3	1.3	2.72	905	1142	1051	0.920	1.26
SSTCC-D150-a	149.7	1.63	4.67	1305	1759	1650	0.938	1.35
SSTCC-D150-b	149.8	1.67	6.43	1305	1790	1666	0.931	1.37
SSTCC-D150-c	150.2	1.67	3.86	1305	1812	1674	0.924	1.39
CFSST-D150-a	150.1	1.68	2.81	1305	1698	1544	0.910	1.30
CFSST-D150-b	149.8	1.65	2.83	1305	1661	1530	0.921	1.27
SSTCC-D180-a	180.8	1.68	4.14	1730	2340	2275	0.972	1.35
SSTCC-D180-b	180.6	1.65	3.94	1730	2333	2257	0.968	1.35
SSTCC-D180-c	180.7	1.67	4.25	1730	2360	2269	0.961	1.36
CFSST-D180-a	180.7	1.69	2.08	1730	2169	2109	0.972	1.25
CFSST-D180-b	180.7	1.7	2.25	1730	2193	2113	0.963	1.27

346 Note: Δ_u is the displacement corresponding to the load-carrying capacity; N_{ue} is the capacity of experimental
 347 results; N_{s+c} is the sum capacity of steel and concrete; N_c is the calculated capacity of specimen.

348 6. Conclusions

349 This paper studied the behavior of axially loaded stainless steel tube confined concrete stub columns

350 and concrete-filled stainless steel stub columns. The experimental phenomena are introduced in detail.

351 Based on the analysis of experimental results, the following conclusions can be drawn:

352 (1) Both stainless steel tube confined concrete stub columns and concrete-filled stainless steel stub
353 columns possess high load-carrying capacity. The load-carrying capacity of stainless steel tube confined
354 concrete members is higher than that of concrete-filled stainless steel stub columns.

355 (2) The quality of welding is a key factor for steel tube confined specimens, which would influence
356 the deformation ability of the specimens. The seamless steel tubes are suggested to be used for stainless
357 steel tube confined concrete members.

358 (3) For stainless steel tube confined concrete members, although the stainless steel stub is cut on both
359 ends, the steel tube would still resist certain percentage of the overall vertical load. Based on the test results,
360 the contribution of axial stress of steel tube to the load-carrying capacity should be considered.

361 (4) A formula to calculate the load-carrying capacity of stainless steel tube confined concrete members
362 is proposed, which is also can be used to calculate the load-carrying capacity of concrete-filled stainless
363 steel stub columns.

364 **Acknowledgements**

365 This research was financially supported by the Jilin Science and Technology Development Project
366 (20180201031SF), the Major (key) Projects of Key R & D Projects in the Ningxia Hui Autonomous Region
367 (2018BEG02009) and the National Natural Science Foundation of China (Grant No. 51778185). The
368 authors wish to acknowledge the sponsors. However, any opinions, findings, conclusions and
369 recommendations presented in this paper are those of the authors and do not necessarily reflect the views of
370 the sponsors.

371 **References**

- 372 [1] Liu Jiepeng, Zhang Sumei. Behavior and strength of circular tube confined reinforced-concrete
373 (CTRC) columns. *Journal of Constructional Steel Research*, 2009, 65: 1447-1458.
- 374 [2] Wang Xuanding, Liu Jiepeng, Zhang Sumei. Behavior of short circular tubed-reinforced-concrete
375 columns subjected to eccentric compression. *Engineering Structures*, 2015, 105:77-86.
- 376 [3] Liu Jiepeng, Zhou Xuhong. Behavior and strength of tubed RC stub columns under axial compression.
377 *Journal of Constructional Steel Research*. 2010, 66:28-36.
- 378 [4] Mcateer Peter, Bonacci F., Lachemi Mohamed. Composite response of high-strength concrete
379 confined by circular steel tube. *ACI Structural Journal*, 2004, 101(5):466-474.
- 380 [5] Hong Mei, Kiiouisis, Ehsani MR, Saadatmanesh H. Confinement effects on high-strength concrete.
381 *ACI Structural Journal*, 2001, 98(4):548-553.
- 382 [6] Liu Faqi, Yang Hua, Leroy Gardner. Post-fire behaviour of eccentrically loaded reinforced concrete
383 columns confined by circular steel tubes. *Journal of Constructional Steel research*, 2016, 122:495-510
- 384 [7] Liu Jiepeng, Teng Yue, Zhang Yusong, et al. Axial stress-strain behavior of high-strength concrete
385 confined by circular thin-walled steel tubes. *Construction and Building Materials*, 2018, 177: 366-377.
- 386 [8] Liu Faqi, Leroy Gardner, Yang Hua. Post-fire behaviour of reinforced concrete stub columns confined
387 by circular steel tubes. *Journal of Constructional Steel Research*, 2014, 102:82-103.
- 388 [9] Wang Xuanding, Liu Jiepeng, Zhou Xuhong. Behaviour and design method of short square
389 tubed-steel-reinforced-concrete columns under eccentric loading. *Journal of Constructional Steel*
390 *Research*, 2016, 116:193-203.
- 391 [10] Liu Jiepeng, Wang Xuanding, Zhang Sumei. Behavior of square tubed reinforced-concrete short
392 columns subjected to eccentric compression. *Thin-Walled Structures*, 2015, 91:108-115.

- 393 [11] Zhou Xuhong, Yan Biao, Liu Jiepeng. Behavior of square tubed steel reinforced-concrete (SRC)
394 columns under eccentric compression. *Thin-Walled Structures*, 2015, 91:129-138.
- 395 [12] Young B, Ellobody E. Experimental investigation of concrete-filled coldformed high strength stainless
396 steel tube columns. *Journal of Constructional Steel Research*, 2006, 62(5):484–492.
- 397 [13] Ellobody E, Young B. Design and behavior of concrete-filled cold-formed stainless steel tube columns.
398 *Thin-Walled Structures*, 2007, 45(3):259-273.
- 399 [14] Ellobody E, Young B. Design and behaviour of concrete-filled cold-formed stainless steel tube
400 columns. *Engineering Structures*, 2006, 28:716–728.
- 401 [15] Dennis Lam, Leroy Gardner. Structural design of stainless steel concrete filled columns. *Journal of*
402 *Constructional Steel Research*, 2008, 64(11):1275-1282.
- 403 [16] Hassanein, M.F., Kharoob O.F. and Liang Q.Q. Circular concrete-filled double skin tubular short
404 columns with external stainless steel tubes under axial compression. *Thin-Walled Structures*, 2013,
405 73:252-263.
- 406 [17] Suliman Abdalla, Farid Abed, Mohammad AlHamaydeh. Behavior of CFSTs and CCFSTs under
407 quasi-static axial compression. *Journal of Constructional Steel Research*, 2013, 90(5):235-244.
- 408 [18] Ye Yong, Zhang Shijiang, Han Linhai, et al. Square concrete-filled stainless steel/carbon steel
409 bimetallic tubular stub columns under axial compression. *Journal of Constructional Steel Research*,
410 2018, 146:49-62.
- 411 [19] Han Linhai, Ren Qingxin, Li Wei. Tests on stub stainless steel–concrete–carbon steel double-skin
412 tubular (DST) columns. *Journal of Constructional Steel Research*, 2011, 67(3):437-452.
- 413 [20] Wang Facheng , Han Linhai, Li Wei. Analytical behavior of CFDST stub columns with external
414 stainless steel tubes under axial compression. *Thin-Walled Structures*, 2018, 127: 756-768.

- 415 [21] Feng Ran, Chen Yu, Wei Jiangang, et al. Experimental and numerical investigations on flexural
416 behaviour of CFRP reinforced concrete-filled stainless steel CHS tubes. *Engineering Structures*, 2018,
417 156: 305-321.
- 418 [22] Chen Yu, Feng Ran, Shao Yongbo, et al. Bond-slip behaviour of concrete-filled stainless steel circular
419 hollow section tubes. *Journal of Constructional Steel Research*, 2017, 130:248-263.
- 420 [23] Chen Yu, Wang Kai, Feng Ran, et al. Flexural behaviour of concrete-filled stainless steel CHS
421 subjected to static loading. *Journal of Constructional Steel Research*, 2017, 139:30-43.
- 422 [24] Chen Yu, Feng Ran, Wang Lipeng. Flexural behaviour of concrete-filled stainless steel SHS and RHS
423 tubes. *Engineering Structures*, 2017, 134:159-171.
- 424 [25] GB/T 228-2002. *Metallic materials-Tensile testing at ambient temperature*. Beijing, China; 2002
- 425 [26] GB/T 50081-2002. *Standard for test method of mechanical properties on ordinary concrete*. Beijing,
426 China; 2002.
- 427 [27] Quah W M, Teng J G, Chung K F. Three-Stage Full-Range stress-Strain Model for Stainless Steels.
428 *Journal of Structural Engineering ASCE*, 2008, 134 (9):1518-1527.
- 429 [28] Zhang Sumei, Guo Lanhui, Ye Zaili and Wang Yuyin. Behavior of steel tube and confined high
430 strength concrete for concrete-filled RHS tubes. *Advances in Structural Engineering*, 2005,
431 8(2):101-116.
- 432 [29] Mander JB, Priestley MJN, Park R. Theoretical stress-strain model for confined concrete. *Journal of*
433 *the Structural Engineering*, 1988, 114(8):1804-1826.
- 434